Negative differential thermal conductance by photonic transport in electronic circuits

Shobhit Saheb Dey [*]

Department of Physics, Indian Institute of Technology Kharagpur, Kharagpur 721302, India
and Quantum Research Center, Technology Innovation Institute, Abu Dhabi 9639, UAE

Giuliano Timossi

NEST Istituto Nanoscienze-CNR and Scuola Normale Superiore, I-56127 Pisa, Italy

Luigi Amico [†]

Quantum Research Center, Technology Innovation Institute, Abu Dhabi 9639, UAE;
Centre for Quantum Technologies, National University of Singapore, 3 Science Drive 2, Singapore 117543;
INFN-Sezione di Catania, Via S. Sofia 64, 95127 Catania, Italy;
and MajuLab, CNRS-UNS-NUS-NTU International Joint Research Unit, UMI 3654, Singapore

Giampiero Marchegiani

Quantum Research Center, Technology Innovation Institute, Abu Dhabi 9639, UAE

The negative differential thermal conductance (NDTC) provides the key mechanism for realizing thermal transistors. This exotic effect has been the object of an extensive theoretical investigation, but the implementation is still limited to a few specific physical systems. Here, we consider a simple circuit of two electrodes exchanging heat through electromagnetic radiation. We theoretically demonstrate that the existence of an optimal condition for power transmission, well known as impedance matching in electronics, provides a natural framework for engineering NDTC: the heat flux is reduced when the temperature increase is associated to an abrupt change of the electrode's impedance. As a case study, we numerically analyze a hybrid structure based on thin-film technology, in which the increased resistance is due to a superconductor-resistive phase transition. For typical metallic superconductors operating below 1 K, NDTC reflects in a temperature drop of the order of a few mK by increasing the power supplied to the system. Our numerical work draws new routes for implementing a thermal transistor in nanoscale circuits.

I. INTRODUCTION

The development of quantum technologies is one of the main driving forces of the current physical research [1,2]. In many implementations of this discipline, device miniaturization and low noise requirement have motivated an intense theoretical investigation and experimental activity on thermal transport in nanoscale solid-state devices [3–9]. In this direction, as a combined effect of nonequilibrium thermal fluctuations and nonlinear response, physical systems in which the heat flow $\dot{Q}$ decreases by increasing temperature gradients, i.e., $d\dot{Q}/dT < 0$, can be realized. In these regimes, the system is characterized by a negative differential thermal conductance (NDTC) [10]. Exploring the physical meaning of the NDTC regime defines a certainly interesting line of basic research [11–14]. At the same time, such an effect allows one to configure and fabricate new devices based on NDTC. An

important case study in this context is provided by the thermal transistor introduced 17 years ago by Casati and co-workers [10]. Over the years, several proposals for the implementation of thermal transistors and similar devices have been put forward, with technologies ranging from phononics [15], superconducting junctions [16,17], and electrochemical cells [18] to near-field devices [19–23]. Even though great efforts have been devoted to the problem, engineering of NDTC in physical systems is still a challenging task, with only few experimental observations in specific systems being carried out [24–26]. In our work, we will show how a circuit approach to photon-mediated thermal transport can provide a general route for NDTC engineering. In our logic, we rely on a specific "resonant" property holding for the thermal transmission: the electromagnetic power turns out to be optimally transmitted between two circuital elements if a certain impedance matching condition is fulfilled [27]. Starting from this condition, we impart an abrupt impedance mismatch by a temperature change. We shall see that such protocol can lead to NDTC. After a general discussion of the mechanism, we present a quantitative investigation in a realistic platform in which the impedance mismatch is achieved through the

───────
[*]shobhitsahebdey@iitkgp.ac.in
[†]On leave from the Dipartimento di Fisica e Astronomia "Ettore Majorana", University of Catania.
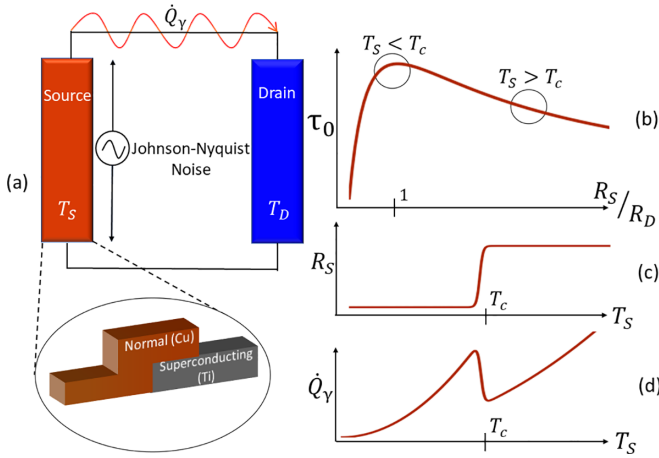
FIG. 1. NDTC in photonic transport. (a) Circuit scheme: source and drain electrode are connected through a lossless line. In the presence of a thermal gradient, heat is transferred through a photon-mediated mechanism. In the blow-up, we show the implementation discussed in the second part of the manuscript, where the source is given as a series of a normal metal and a superconductor. (b) Power transfer coupling coefficient between two normal resistors R_S and R_D. The transmission is maximum for $R_S = R_D$ (impedance matching condition). (c) Sharp increase of the source resistance due to a phase change occurring at the temperature T_c. (d) Resulting NDTC in the photon-mediated heat current.

normal-to-superconductor phase transition. We note that the photonic heat transport between two normal metals has been recently investigated in different experiments [28–33], where superconducting elements are exploited to realize a tunable coupling, both in the classical and in the quantum regime [32,34]. Here, we investigate photon-mediated heat transport in superconductors that, because of their impedance's strong temperature dependence, provide important examples of coherent networks in which nonlinear transport effects can take place [23,35–38].

II. MODEL

We consider the scheme depicted in Fig. 1(a). The system is composed of two electrodes, denoted as source (S) and drain (D), electrically connected through wires of negligible losses. We assume that the lead S is in thermal equilibrium with temperature T_S, while the drain resides at temperature T_D. When a thermal gradient is present, i.e., for $T_S \neq T_D$, heat is exchanged between the two elements. With a properly studied design detailed below, the heat transfer between the source and the drain is dominated by the photonic channel while competing mechanisms are negligible; we comment more extensively on this point in the second part of this work. Radiative heat transfer is typically investigated in the framework of fluctuation electrodynamics, which phenomenologically combines quantum and thermal fluctuations with the Maxwell equations describing the electromagnetic fields [39–41]. For the sake of generality, we follow a lumped parameters approach valid at low temperatures for thermal photons wavelengths (λ_T) larger than the size of the typical circuit element. In other words, the source, the drain, and the superconducting wires have physical dimensions much shorter than the

photon thermal wavelength $\lambda_T = 2\pi \hbar c/(k_B T)$ (with $\hbar$ the reduced Planck's constant, k_B the Boltzmann constant, and c the speed of light), which is 1.4 cm at $T = 1$ K. In this regime, we can follow the circuit approach of Ref. [42] to determine the radiative heat transfer. Due to the quantum and thermal fluctuations of charges, a voltage noise across the ends of the source electrode, called the Johnson-Nyquist noise [43,44], occurs. The power spectrum of this noise is characterized by the fluctuation-dissipation theorem [45] and is given as $S_V(\omega) = 4\hbar\omega \, \mathrm{Re}\,[Z_S(\omega, T_S)][n(\hbar\omega, T_S) + 1/2]$, where ω is the angular frequency of fluctuation, $n(\epsilon, T) = [e^{\epsilon/(k_B T)} - 1]^{-1}$ is the Bose-Einstein distribution, and $Z_S(\omega, T_S)$ is the source's impedance. The photons emitted due to fluctuations in the source are absorbed by the drain electrode. In the circuit approach, this effect manifests itself as joule heating of the drain electrode due to the current produced by the Johnson-Nyquist voltage noise. Spectrum of the corresponding noise current in the circuit is obtained by applying the Kirchhoff laws and reads $S_I(\omega) = S_V(\omega)/|Z_{tot}|^2$, where $Z_{tot} = Z_S(\omega, T_S) + Z_D(\omega, T_D)$ is the total impedance of the circuit. Hence the spectrum of power dissipated in the drain is $S_P(\omega) = \mathrm{Re}\,[Z_D(\omega, T_D)]S_I(\omega)$. The total power transferred is obtained by integrating over the angular frequencies ω, giving

$$\dot{Q}_{S \to D}(T_S, T_D) = \int_0^\infty \frac{\hbar\omega}{2\pi} \tau(\omega, T_S, T_D) \left[n(\hbar\omega, T_S) + \frac{1}{2} \right] d\omega, \quad (1)$$

where the effective photon transmission coefficient has been identified as [42,44,46]

$$\tau(\omega, T_S, T_D) = 4 \frac{\mathrm{Re}[Z_S(\omega, T_S)]\mathrm{Re}[Z_D(\omega, T_D)]}{|Z_S(\omega, T_S) + Z_D(\omega, T_D)|^2}. \quad (2)$$

The heat transfer rate in Eq. (1) represents the total power radiated by the source and transmitted to the drain, without accounting for the heat back-flow due to electromagnetic fluctuations in the drain electrode. The net power transmitted is then obtained by subtracting the heat current $\dot{Q}_{D \to S}$ flowing from the drain to the source, i.e., $\dot{Q}_\gamma = \dot{Q}_{S \to D} - \dot{Q}_{D \to S}$. Due to symmetry, $\dot{Q}_{D \to S}$ is simply obtained by exchanging $S \leftrightarrow D$ in Eq. (1), yielding the following expression for $\dot{Q}_\gamma$ [28,42]:

$$\dot{Q}_\gamma(T_S, T_D) = \int_0^\infty \frac{\hbar\omega}{2\pi} \tau(\omega, T_S, T_D)[n(\hbar\omega, T_S) - n(\hbar\omega, T_D)] \, d\omega. \quad (3)$$

In this setting, a NDTC can be achieved, for instance, when $\dot{Q}_\gamma$ *decreases* by increasing T_S for a fixed value of $T_D < T_S$. To give a simplified view, we first discuss the case where the source impedance Z_S has no reactive components and does not depend on the photon energy, i.e., $Z_S(\omega, T_S) = R_S(T_S)$. For the drain, we consider here and in the rest of the manuscript a normal metal resistor, independent on the drain temperature T_D, i.e., $Z_D(\omega, T_D) = R_D$. In this case, the integral in Eq. (3) can be explicitly evaluated as $\dot{Q}_\gamma(T_S, T_D) = \tau_0(R_S/R_D)\pi k_B^2(T_S^2 - T_D^2)/(12\hbar)$, where $\tau_0(x) = 4x/(x+1)^2$. In this expression the T^2 dependence of the heat current expresses blackbody radiation in 1D, characterized by a modified Stefan-Boltzmann

constant $\sigma_{SB}^{1D} = \pi k_B^2/(6\hbar)$ [47,48]. The one-dimensional nature of the transport stems from the topology of the electrical circuit which connects the two elements, where the radiated photons are transmitted. The coupling coefficient τ_0 characterizes the efficiency of the power transmission, related to the relative dissipation in each element.

The key property that we use to engineer the NDTC is the nonmonotonous behavior of the transmission τ_0 as a function of the resistance ratio (R_S/R_D); in particular, τ_0 results in being maximum at the impedance matching condition, i.e., for $R_S = R_D$ [42]. This result is also known in the literature as the maximum power transfer theorem: it expresses a general statement on optimal power transfer between two elements, ranging from mechanical collisions to electromagnetic phenomena (such as the one investigated here) [49,50]. We consider a source electrode characterized by a resistance which depends sharply on the temperature around the critical value T_c, i.e., $R_S = R_D$ for $T < T_c$ and $R_S \gg R_D$ for $T > T_c$ [see Fig. 1(c)]. As a consequence, the transmission τ_0 is reduced from unity (for $T < T_c$, being $R_S = R_D$) to a value much smaller than one ($T > T_c$, with $R_S/R_D \gg 1$) when the temperature is increased from $T < T_c$ to $T > T_c$, hence making $\dot{Q}_\gamma$ decrease by increasing T_S in the vicinity of T_c—Fig. 1(d). Note that at larger values of the source temperature the heat conductance is again positive, with the transmission being approximately constant for $T > T_c$.

III. CASE STUDY: SUPERCONDUCTING THIN FILMS

Now we discuss a possible scheme for the detection and implementation of NDTC. To mimic the sharp resistance increase of Fig. 1(c), we exploit a superconducting to normal phase transition [51]. We assume the source is composed of a series of a normal element (with resistance $R_N = R_D$ to ensure impedance matching) and a superconducting element, connected through a clean contact of negligible resistance [see Fig. 1(a)] [52]. The clean contact can be achieved through electrode beam evaporation of the two films in a ultra-high-vacuum chamber. Below the superconducting critical temperature, the dissipation in the superconductor is negligible, giving $\mathrm{Re}\,[Z_S(\omega, T_S)] \sim R_D$, whereas $\mathrm{Re}\,[Z_S(\omega, T_S)] = R_D + R_0$ for $T > T_c$, where R_0 is the resistance of the superconducting element in the normal state. We choose to operate in the sub-kelvin regime, where the photonic heat current is more relevant to the thermal equilibration [36,38,44]. On the material side, we consider thin metallic films which can be deposited through electron-beam evaporation, such as titanium (Ti) as the superconductor (with typical critical temperature in the range 0.3–0.5 K [53,54], we set $T_c = 0.4$ K in our calculations) and copper (Cu) for the normal conducting elements. The wires can be realized with superconducting aluminum (Al) or niobium (Nb), which displays higher critical temperature than Ti [55], and therefore can account for realizing lossless lines. Indeed, at low temperatures, the superconducting gap exponentially suppresses both ac losses and the source-to-drain heat conduction by quasiparticles [56], which may otherwise overcome the photonic transport due to the galvanic connection between the source and drain in our setup [see Fig. 1(a)]. At the same time, the direct conduction of heat between the electrodes and the wire is suppressed

by Andreev mirroring [38]. As a result, the heat transfer is dominated by the photonic radiation of Eq. (3) in the relevant temperature range, as also experimentally demonstrated in Ref. [56]. For simplicity, we neglect the interfacial resistance between the wire and the two electrodes: this resistance reduces the transmitted heat current by increasing the real part of Z_{tot}, but does not significantly affect the phenomenology discussed below. Finally, reactive contributions to the photonic transport due to the kinetic inductance of the wire can be made negligible with a suitable geometry design; typical phase-shift effects of long waveguides [57] are negligible due to the size of the superconducting wire, much smaller than the photon thermal wavelength (of the order of centimeters or larger).

A. Complex impedance of the superconducting thin film

We start by discussing the photon-mediated heat transport. In our setup, the impedance of the two leads are $Z_S(\omega, T_S) = R_D + Z_0(\omega, T_S)$ and $Z_D = R_D$. As recently experimentally demonstrated [54], the complex impedance of Ti can be modeled within the Mattis-Bardeen theory [58], valid for Bardeen-Cooper-Schrieffer (BCS) superconductors. More precisely, the complex impedance reads $Z_0(\omega, T_S) = R_0[\sigma_1(\omega, T_S) - \iota\sigma_2(\omega, T_S)]^{-1}$, where the real ($\sigma_1$) and the imaginary ($\sigma_2$) parts of the complex conductivity (scaled to the normal conductivity) are expressed by

$$\sigma_1(\omega, T) = \frac{2}{\hbar\omega} \int_\Delta^\infty \nu(E, E')[f(E, T) - f(E', T)]\,dE$$
$$- \frac{\Theta(\hbar\omega - 2\Delta)}{\hbar\omega} \int_{\Delta-\hbar\omega}^{-\Delta} \nu(E, E')[1 - 2f(E', T)]\,dE,$$
$$(4)$$

$$\sigma_2(\omega, T) = \frac{1}{\hbar\omega} \int_{-\Delta,\Delta-\hbar\omega}^{\Delta} |\nu(E, E')|[1 - 2f(E', T)]\,dE.$$
$$(5)$$

Above, $\Theta(x)$ is the Heaviside-step function, $E' = E + \hbar\omega$, and $f(E, T) = [e^{E/(k_B T)} + 1]^{-1}$ is the Fermi function. In Eq. (5), the lower limit of the integral is the maximum between $-\Delta$ or $\Delta - \hbar\omega$; in other words, the lower limit is $-\Delta$, $\Delta - \hbar\omega$ for $\hbar\omega > 2\Delta$, and $\hbar\omega < 2\Delta$, respectively. We introduced the function [59]

$$\nu(E, E') = \frac{EE' + \Delta^2}{\sqrt{E^2 - \Delta^2}\sqrt{E'^2 - \Delta^2}}. \quad (6)$$

The superconducting gap is approximately given by $\Delta(T) = \Delta_0 \tanh(1.74\sqrt{T_c/T - 1})$ [60] for $T \leqslant T_c$ ($\Delta=0$ for $T \geqslant T_c$), where $\Delta_0 = 1.76 k_B T_c$, according to the BCS theory. The dissipative processes in the superconductor are given by thermally excited quasiparticles [first integral of Eq. (4)] or through pair-breaking processes due to photon absorption that may occur for $\hbar\omega > 2\Delta$ [second integral of Eq. (4)]. The imaginary part of the conductivity Eq. (5) gives the kinetic inductance of the superconducting film.

B. Temperature dependence of the heat current

Figure 2(a) displays $\dot{Q}_\gamma$ as a function of the source temperature T_S, for $T_D = 30$ mK and different values of the ratio
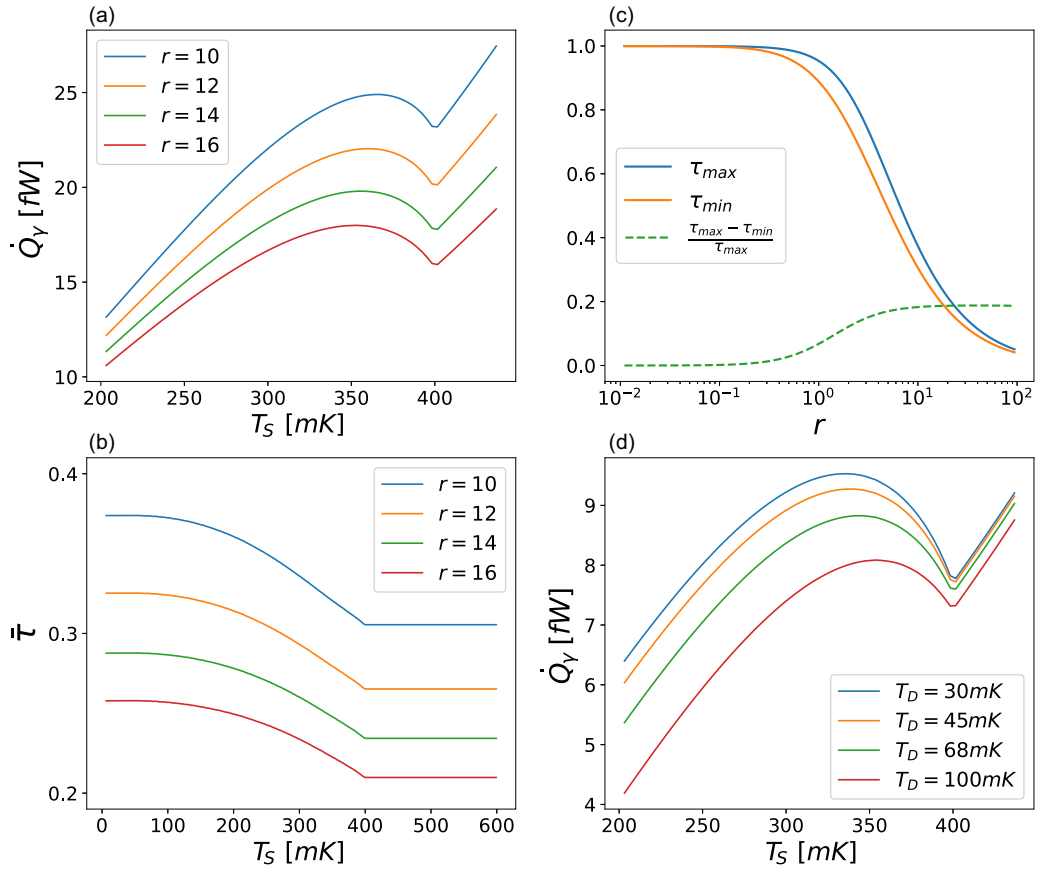
FIG. 2. NDTC in the specific implementation based on low-temperature superconductors. (a) $\dot{Q}_\gamma$ vs T_S with $T_D = 30$ mK for different values of $r = R_0/R_D$. NDTC appears for source temperatures T_S around (350 mK, 400 mK). (b) Energy averaged thermal transmission $\bar{\tau}$ vs T_S for the same values of r as in (a). (c) $\tau_{\max}$, $\tau_{\min}$ and their relative difference as function of r showing favorable operating region to observe NDTC. (d) $\dot{Q}_\gamma$ vs T_S for $r = 36$ and different values of T_D.

$r = R_0/R_D$. Notably, the evolution is nonmonotonic with T_S and the system displays NDTC for source temperatures approximately in the range around [350 mK, 400 mK]. Upon increasing R_0, the photonic heat current decreases. Here the reduction of $\dot{Q}_\gamma$ with R_0 for $T > T_c$ arises from suppression of $\tau_0(x)$ for $x > 1$, while for $T < T_c$ it is related to the imaginary part of the $Z_S(\omega, T_S)$, i.e., kinetic inductance. To analyze such a feature, we focus on the temperature dependence of τ. We define an average transmission $\bar{\tau}(T_S) = \hbar(2\Delta_0)^{-1} \int_0^{2\Delta_0/\hbar} \tau(\omega, T_S) d\omega$ [61]. Figure 2(b) displays $\bar{\tau}$ as a function of the source temperature T_S, for the same values of r as in Fig. 2(a). The transmission is monotonically decreasing with T_S, being maximum at $T_S \ll T_c$, i.e., $\tau_{\max} = \bar{\tau}(T_S \to 0)$, and constant for $T_S \gtrsim T_c$, with $\tau_{\min} = 4(1 + r)/(2 + r)^2$. Differently from the idealized situation displayed in Fig. 1, $\tau < 1$ even at low temperatures. This behavior is due to the non-negligible kinetic inductance of the superconductor, which reduces τ [see Eq. (2)]. Hence, even though an increase of R_0 turns out always beneficial in the schematics of Fig. 1(b), in the realistic case, an arbitrarily large value of R_0 may hinder the NDTC behavior as also seen in Fig. 2(a). Indeed, $\tau_{\max}$ and $\tau_{\min}$ decreases monotonically as a function of r, as displayed in Fig. 2(c) (solid curves). Notably, the relative transmission modulation, defined as $(\tau_{\max} - \tau_{\min})/\tau_{\max}$, grows monotoni-

cally with r and it is approximately saturating to $1 - 8/\pi^2 \sim 0.19$ for $r \sim 10$ [see dashed curve in Fig. 2(c)] [62]. As a result, the phenomenology of NDTC is well displayed for values of r in the range [10,100].

In Fig. 2(d), we display $\dot{Q}_\gamma$ as a function of T_S for $r = 36$ and different values of T_D. For a given value of the source temperature, the heat current typically decreases by increasing T_D, due to the reduction of the thermal gradient. Notably, the NDTC phenomenology for source temperatures $T_S \lesssim T_c$ is robust even with a sizable change of the drain temperature. This feature is crucial for the detection of the NDTC discussed below.

C. Thermal schematic and self-consistent calculation

In the above computations, we characterized the photon-mediated thermal transport as a function of the temperatures of the source for selected values of the drain temperature. However, in an actual experiment, the temperatures T_S and T_D are not directly controlled. Instead, power is injected into the system and the temperatures T_S, T_D are the result of the power balance in each electrode [9]. In experiments based on hybrid-normal superconducting thin films, power is typically injected by joule heating; in other words, two normal (or superconducting) electrodes are coupled to the source through
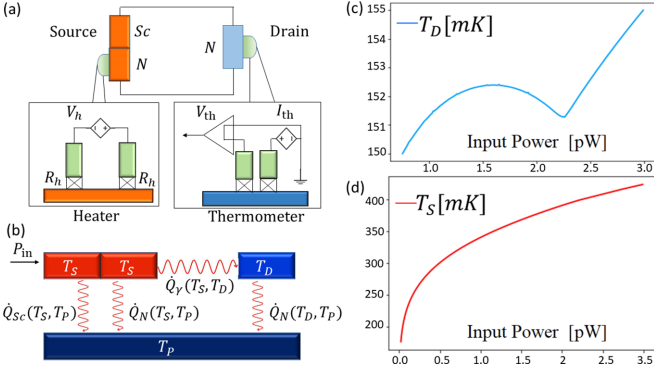
FIG. 3. Thermal balance and source and drain steady-state temperatures. (a) Schematics showing typical configuration for power injection in the source electrode (heater) and thermometry with additional electrodes tunnel coupled to the source and the drain. (b) Heat flow diagram: input power is provided to the source using externally controlled voltage source providing joule heating and losses due to electron-phonon coupling are included. (c) Steady-state temperature of the drain T_D vs input power P_{in}, showing negative differential characteristics with respect to P_{in}. (d) Steady-state temperature of the source T_S vs P_{in}, showing a monotonic increase with input power. Parameters: $T_p = 30$ mK, $\rho_{Cu} = 3$ μΩ cm [70], $l_{Cu} = 2$ μm, $\mathcal{A}_{Cu} = 700 \times 30$ nm^2, $\rho_{Ti} = 30$ μΩ cm [71], $l_{Ti} = 6$ μm, and $\mathcal{A}_{Ti} = 700 \times 25$ nm^2, where $\rho, l, \mathcal{A}$ are the normal state resistivity, the length, and the cross section of the films, respectively.

an insulating barrier [see schematic for the heater in Fig. 3(a)]. Applying a bias voltage V_h between the two electrodes in the heater, power $\sim V_h^2/4R_h$ (with R_h tunneling resistance of each barrier) is dissipated in the source [63], locally raising the quasiparticle temperature. The drain temperature can be measured via tunnel junction thermometry [3,64–67]; two superconducting electrodes are coupled to the drain electrode via strongly oxidized barriers (to prevent additional heat losses) and supplied with a bias current I_{th} [schematic in Fig. 3(a)]. After calibration, the voltage drop across the structure (V_{th}) gives the temperature of the (normal) drain electrode. This measurement scheme is insensitive to the temperature of the superconducting elements for $T_D \leqslant 0.4T_c^{th}$; for our parameters' value this inequality holds for a thermometer electrode based on superconducting aluminum ($T_c^{th} \approx 1.2$ K is the critical temperature of the thermometer).

The thermal exchanges in our system are schematically depicted in Fig. 3(b). Experiments based on low-temperature superconducting thin films are typically well described within the quasiequilibrium regime [3,6]. Namely, in each electrode, quasiparticles and phonons can be treated as separate subsystems, which may thermalize to different temperatures, since the electron-phonon scattering rate slows down at very low temperatures. We assume that the phonons in each part of the device are well thermalized to the substrate temperature ($T_p \sim 30$ mK set by the cryogenic dilution fridge) due to the vanishing Kapitza resistance between the substrate and thin metallic films [3,9]. Thus, in our modeling, the phonons do not contribute to the heat transfer between the source and drain; nevertheless, the electron-phonon interaction plays a central role in the thermalization of the two electrodes, as detailed below. Due to the clean contact between Ti and Cu,

we neglect any potential small thermal gradient in the source electrode, characterizing the electron (in the normal metal) and the quasiparticle (in the superconductor) subsystem with a single temperature T_S. This approximation is valid for layers with dimensions smaller than the thermal healing length associated with electron-phonon interaction, which we estimate in the range of tens to hundreds of μm [3]. The electronic temperature of the drain is given by T_D. When power P_{in} is injected in the source, the source temperature increases $T_S > T_p$, producing photon-mediated exchange $\dot{Q}_\gamma$ with the drain. At the same time, heat is exchanged with the phononic bath both in the normal ($\dot{Q}_N$) and in the superconducting ($\dot{Q}_{Sc}$) parts of the device. At the steady-state condition, in each element the ingoing heat current must be equal to the outgoing heat current, giving

$$P_{in} = \dot{Q}_\gamma(T_S, T_D) + \dot{Q}_N(T_S, T_p) + \dot{Q}_{Sc}(T_S, T_p),$$
$$\dot{Q}_\gamma(T_S, T_D) = \dot{Q}_N(T_D, T_p). \tag{7}$$

The electron-phonon coupling in each Cu lead is given by $\dot{Q}_N(T, T_p) = \Sigma_{Cu}\mathcal{V}_N(T^5 - T_p^5)$, where $\mathcal{V}_N$ is the volume of each copper electrode and $\Sigma_{Cu} = 3 \times 10^9$ W m^{-3}K^{-5} is the material dependent electron-phonon coupling constant [3]. For the superconductor, the electron-phonon interaction reads [68,69]

$$\dot{Q}_{Sc}(T_S, T_p) = \alpha_s \int_0^\infty d\epsilon\, \epsilon^3 [n(\epsilon, T_S) - n(\epsilon, T_p)]\mathcal{F}(\epsilon, T_S), \tag{8}$$

where $\alpha_s = \Sigma_{Ti}\mathcal{V}/[24\zeta(5)k_B^5]$ and

$$\mathcal{F}(\epsilon, T_S) = \int_{-\infty}^\infty dE\, \rho(E)\rho(E')\left(1 - \frac{\Delta^2}{EE'}\right)$$
$$\times [f(E, T_S) - f(E', T_S)], \tag{9}$$

with $E' = E + \epsilon$. Above, $\Sigma_{Ti} = 1.3 \times 10^9$ W m^{-3}K^{-5} is the coupling coefficient [3], $\mathcal{V}$ is the volume of the superconducting lead, $\zeta(z)$ is the Riemann-zeta function, and $\rho(E) = |E|\theta(|E| - \Delta)/\sqrt{E^2 - \Delta^2}$ is the BCS density of states. For given values of the phonon temperature T_p and the input power P_{in} Eq. (7) is a nonlinear system of integroalgebraic equations in the two-variables for T_S and T_D.

Figures 3(b) and 3(c) display the solution of Eq. (7), obtained through a Newton-Raphson optimization algorithm, as a function of the input power P_{in}. Notably, while T_S increases monotonously with P_{in} [see Fig. 3(c)], the drain temperature T_D decreases for input power around the range [1.5,2.25] pW [see Fig. 3(b)]. This behavior is a signature of NDTC in the photonic channel. Indeed, when T_S is close to T_c (400 mK) the heat exchange is reduced by increasing P_{in}, in agreement with our previous discussion, resulting in a decrease of T_D due to the second equation in Eq. (7).

IV. CONCLUSIONS

In summary, we investigated the negative differential thermal conductance (NDTC) in the photonic heat transport between two electrodes, within a lumped circuital approach. We rely on a photon resonant transmission that, in analogy of the electronic principle of impedance matching [27], minimizes the loss in the heat transmission. We demonstrated how

such resonant transmission can be exploited as a reference point to realize NDTC. An abrupt impedance mismatch causes a reduction of the heat flow that can be transmitted among the two electrodes and therefore the differential conductance is negative. In the second part of the paper, we focus on a specific design based on low-temperature superconductor that can be realized with the state-of-the-art nanofabrication techniques. Our calculations show that the effect leads to temperature drops larger than 1 mK. Thus the predicted NDTC phenomenology can be identified with well-established normal-insulator-superconductor junction thermometric techniques, with typical uncertainty of 40 μK [29]. Our work provides a general protocol for engineering NDTC in electric circuits

where heat is exchanged through electromagnetic radiation. In this respect, superconducting circuits certainly provide a promising platform. The general nature of the maximum power transfer condition, though, may trigger investigations of NDTC on a wider variety of physical implementations. Improved performance in terms of the operating temperature range or size of the temperature drop with the use of alternative materials and phase transitions. These topics could be the subject of future research.

[1] J. P. Dowling and G. J. Milburn, Quantum technology: the second quantum revolution, Philos. Trans. R. Soc. A **361**, 1655 (2003).

[2] A. Acín, I. Bloch, H. Buhrman, T. Calarco, C. Eichler, J. Eisert, D. Esteve, N. Gisin, S. J. Glaser, F. Jelezko *et al.*, The quantum technologies roadmap: A european community view, New J. Phys. **20**, 080201 (2018).

[3] F. Giazotto, T. T. Heikkilä, A. Luukanen, A. M. Savin, and J. P. Pekola, Opportunities for mesoscopics in thermometry and refrigeration: Physics and applications, Rev. Mod. Phys. **78**, 217 (2006).

[4] Y. Dubi and M. Di Ventra, Colloquium: Heat flow and thermoelectricity in atomic and molecular junctions, Rev. Mod. Phys. **83**, 131 (2011).

[5] G. E. W. Bauer, E. Saitoh, and B. J. van Wees, Spin caloritronics, Nat. Mater. **11**, 391 (2012).

[6] J. T. Muhonen, M. Meschke, and J. P. Pekola, Micrometre-scale refrigerators, Rep. Prog. Phys. **75**, 046501 (2012).

[7] D. G. Cahill, P. V. Braun, G. Chen, D. R. Clarke, S. Fan, K. E. Goodson, P. Keblinski, W. P. King, G. D. Mahan, A. Majumdar, H. J. Maris, S. R. Phillpot, E. Pop, and L. Shi, Nanoscale thermal transport. II. 2003-2012, Appl. Phys. Rev. **1**, 011305 (2014).

[8] B. Song, A. Fiorino, E. Meyhofer, and P. Reddy, Near-field radiative thermal transport: From theory to experiment, AIP Adv. **5**, 053503 (2015).

[9] A. Fornieri and F. Giazotto, Towards phase-coherent caloritronics in superconducting circuits, Nat. Nanotechnol. **12**, 944 (2017).

[10] B. Li, L. Wang, and G. Casati, Negative differential thermal resistance and thermal transistor, Appl. Phys. Lett. **88**, 143501 (2006).

[11] N. Yang, N. Li, L. Wang, and B. Li, Thermal rectification and negative differential thermal resistance in lattices with mass gradient, Phys. Rev. B **76**, 020301(R) (2007).

[12] D. He, B.-Q. Ai, H.-K. Chan, and B. Hu, Heat conduction in the nonlinear response regime: Scaling, boundary jumps, and negative differential thermal resistance, Phys. Rev. E **81**, 041131 (2010).

[13] D. He, S. Buyukdagli, and B. Hu, Origin of negative differential thermal resistance in a chain of two weakly coupled nonlinear lattices, Phys. Rev. B **80**, 104302 (2009).

[14] J. Hu and Y. P. Chen, Existence of negative differential thermal conductance in one-dimensional diffusive thermal transport, Phys. Rev. E **87**, 062104 (2013).

[15] N. Li, J. Ren, L. Wang, G. Zhang, P. Hänggi, and B. Li, Colloquium: Phononics: Manipulating heat flow with electronic analogs and beyond, Rev. Mod. Phys. **84**, 1045 (2012).

[16] A. Fornieri, G. Timossi, R. Bosisio, P. Solinas, and F. Giazotto, Negative differential thermal conductance and heat amplification in superconducting hybrid devices, Phys. Rev. B **93**, 134508 (2016).

[17] M. Zare, Negative differential thermal conductance in a borophane normal metal–superconductor junction, Supercond. Sci. Technol. **32**, 115002 (2019).

[18] A. Sood, F. Xiong, S. Chen, H. Wang, D. Selli, J. Zhang, C. J. McClellan, J. Sun, D. Donadio, Y. Cui, E. Pop, and K. E. Goodson, An electrochemical thermal transistor, Nat. Commun. **9**, 4510 (2018).

[19] C. R. Otey, W. T. Lau, and S. Fan, Thermal Rectification through Vacuum, Phys. Rev. Lett. **104**, 154301 (2010).

[20] L. Zhu, C. R. Otey, and S. Fan, Negative differential thermal conductance through vacuum, Appl. Phys. Lett. **100**, 044104 (2012).

[21] P. Ben-Abdallah and S.-A. Biehs, Near-Field Thermal Transistor, Phys. Rev. Lett. **112**, 044301 (2014).

[22] S.-A. Biehs, R. Messina, P. S. Venkataram, A. W. Rodriguez, J. C. Cuevas, and P. Ben-Abdallah, Near-field radiative heat transfer in many-body systems, Rev. Mod. Phys. **93**, 025009 (2021).

[23] E. Moncada-Villa and J. C. Cuevas, Normal-Metal–Superconductor Near-Field Thermal Diodes and Transistors, Phys. Rev. Appl. **15**, 024036 (2021).

[24] M. A. Kats, R. Blanchard, S. Zhang, P. Genevet, C. Ko, S. Ramanathan, and F. Capasso, Vanadium Dioxide as a Natural Disordered Metamaterial: Perfect Thermal Emission and Large Broadband Negative Differential Thermal Emittance, Phys. Rev. X **3**, 041004 (2013).

[25] K. Ito, K. Nishikawa, H. Iizuka, and H. Toshiyoshi, Experimental investigation of radiative thermal rectifier using vanadium dioxide, Appl. Phys. Lett. **105**, 253503 (2014).

[26] V. Musilová, T. Králík, T. Fořt, and M. Macek, Strong suppression of near-field radiative heat transfer by superconductivity in nbn, Phys. Rev. B **99**, 024511 (2019).

[27] C. J. Kikkert, *RF Electronics: Design and Simulation* (James Cook University, Townsville, QLD, Australia, 2013).

[28] M. Meschke, W. Guichard, and J. P. Pekola, Single-mode heat conduction by photons, Nature (London) **444**, 187 (2006).

[29] A. Ronzani, B. Karimi, J. Senior, Y.-C. Chang, J. T. Peltonen, C. Chen, and J. P. Pekola, Tunable photonic heat transport in a quantum heat valve, Nat. Phys. **14**, 991 (2018).

[30] J. Senior, A. Gubaydullin, B. Karimi, J. T. Peltonen, J. Ankerhold, and J. P. Pekola, Heat rectification via a superconducting artificial atom, Commun. Phys. **3**, 40 (2020).

[31] O. Maillet, D. Subero, J. T. Peltonen, D. S. Golubev, and J. P. Pekola, Electric field control of radiative heat transfer in a superconducting circuit, Nat. Commun. **11**, 4326 (2020).

[32] G. Thomas, J. P. Pekola, and D. S. Golubev, Photonic heat transport across a Josephson junction, Phys. Rev. B **100**, 094508 (2019).

[33] A. Gubaydullin, G. Thomas, D. S. Golubev, D. Lvov, J. T. Peltonen, and J. P. Pekola, Photonic heat transport in three terminal superconducting circuit, Nat. Commun. **13**, 1552 (2022).

[34] B. Karimi, J. P. Pekola, M. Campisi, and R. Fazio, Coupled qubits as a quantum heat switch, Quantum Sci. Technol. **2**, 044007 (2017).

[35] E. Nefzaoui, K. Joulain, J. Drevillon, and Y. Ezzahri, Radiative thermal rectification using superconducting materials, Appl. Phys. Lett. **104**, 103905 (2014).

[36] R. Bosisio, P. Solinas, A. Braggio, and F. Giazotto, Photonic heat conduction in Josephson-coupled Bardeen-Cooper-Schrieffer superconductors, Phys. Rev. B **93**, 144512 (2016).

[37] J. Ordonez-Miranda, K. Joulain, D. De Sousa Meneses, Y. Ezzahri, and J. Drevillon, Photonic thermal diode based on superconductors, J. Appl. Phys. **122**, 093105 (2017).

[38] G. Marchegiani, A. Braggio, and F. Giazotto, Highly efficient phase-tunable photonic thermal diode, Appl. Phys. Lett. **118**, 022602 (2021).

[39] S. M. Rytov, Theory of electric fluctuations and thermal radiation, Tech. Rep., Air Force Cambridge Research Labs Hanscom AFB MA, 1959 (unpublished).

[40] D. Polder and M. Van Hove, Theory of radiative heat transfer between closely spaced bodies, Phys. Rev. B **4**, 3303 (1971).

[41] J. Wise, Theory of heat transfer in nanostructures: Microscopic and phenomenological approaches, Ph.D. thesis, Université Grenoble Alpes [2020-...], 2021.

[42] L. M. A. Pascal, H. Courtois, and F. W. J. Hekking, Circuit approach to photonic heat transport, Phys. Rev. B **83**, 125113 (2011).

[43] H. Nyquist, Thermal agitation of electric charge in conductors, Phys. Rev. **32**, 110 (1928).

[44] D. R. Schmidt, R. J. Schoelkopf, and A. N. Cleland, Photon-Mediated Thermal Relaxation of Electrons in Nanostructures, Phys. Rev. Lett. **93**, 045901 (2004).

[45] E. M. Lifshitz and L. P. Pitaevskii, *Statistical Physics: Theory of the Condensed State* (Elsevier, Amsterdam, 2013), Vol. 9.

[46] T. Ojanen and A.-P. Jauho, Mesoscopic Photon Heat Transistor, Phys. Rev. Lett. **100**, 155902 (2008).

[47] P. T. Landsberg and A. D. Vos, The stefan-boltzmann constant in n-dimensional space, J. Phys. A: Math. Gen. **22**, 1073 (1989).

[48] The additional factor 1/2 in the heat current is due to the polarization of the photons in the conductors.

[49] M. Harrison, Physical collisions and the maximum power theorem: an analogy between mechanical and electrical situations, Phys. Educ. **48**, 207 (2013).

[50] K. Atkin, Energy transfer and a recurring mathematical function, Phys. Educ. **48**, 616 (2013).

[51] M. Tinkham, *Introduction to Superconductivity* (Dover Publications, Mineola, NY, 2004).

[52] For simplicity, we neglect the superconducting proximity effect between the two elements [72].

[53] M. C. Steele and R. A. Hein, Superconductivity of titanium, Phys. Rev. **92**, 243 (1953).

[54] M. Thiemann, M. Dressel, and M. Scheffler, Complete electrodynamics of a bcs superconductor with μeV energy scales: Microwave spectroscopy on titanium at mk temperatures, Phys. Rev. B **97**, 214516 (2018).

[55] The bulk critical temperature of Al is $T_c^{\mathrm{Al}} = 1.2$ K and larger for thin films (up to 3 K for 3 nm thick films). Bulk niobium has a critical temperature $T_c^{\mathrm{Nb}} = 9.2$ K.

[56] A. V. Timofeev, M. Helle, M. Meschke, M. Möttönen, and J. P. Pekola, Electronic Refrigeration at the Quantum Limit, Phys. Rev. Lett. **102**, 200801 (2009).

[57] M. Partanen, K. Y. Tan, J. Govenius, R. E. Lake, M. K. Mäkelä, T. Tanttu, and M. Möttönen, Quantum-limited heat conduction over macroscopic distances, Nat. Phys. **12**, 460 (2016).

[58] D. C. Mattis and J. Bardeen, Theory of the anomalous skin effect in normal and superconducting metals, Phys. Rev. **111**, 412 (1958).

[59] In Eq. (5), $\sqrt{E^2 - \Delta^2}$ is purely imaginary and should be intended as $\sqrt{\Delta^2 - E^2}$ due to the presence of the absolute value.

[60] This approximate expression gives an accurate description for the temperature dependence of the gap, with an error smaller than 3% for every temperature.

[61] The cutoff at $2\Delta_0/\hbar$ is related to the fact that we are mainly interested in temperatures $T_S \leqslant T_c$.

[62] This value is obtained by integration at $T = 0$, by using the low frequency approximation $Z_0(\omega, T_S = 0) \sim i\hbar\omega R_0/(\pi \Delta_0)$.

[63] Only half of the power is dissipated in the source, thus determining the factor 4 in the denominator (the total tunneling resistance is $2R_h$).

[64] M. Nahum and J. M. Martinis, Ultrasensitive-hot-electron microbolometer, Appl. Phys. Lett. **63**, 3075 (1993).

[65] A. V. Feshchenko, L. Casparis, I. M. Khaymovich, D. Maradan, O.-P. Saira, M. Palma, M. Meschke, J. P. Pekola, and D. M. Zumbühl, Tunnel-Junction Thermometry Down to Millikelvin Temperatures, Phys. Rev. Appl. **4**, 034001 (2015).

[66] H. Courtois, F. W. J. Hekking, H. Q. Nguyen, and C. B. Winkelmann, Electronic coolers based on superconducting tunnel junctions: Fundamentals and applications, J. Low Temp. Phys. **175**, 799 (2014).

[67] B. Karimi, Y.-C. Chang, and J. P. Pekola, Low temperature characteristics of the metal-superconductor nis tunneling thermometer, J. Low Temp. Phys. **207**, 220 (2022).

[68] A. V. Timofeev, C. P. García, N. B. Kopnin, A. M. Savin, M. Meschke, F. Giazotto, and J. P. Pekola, Recombination-Limited Energy Relaxation in a Bardeen-Cooper-Schrieffer Superconductor, Phys. Rev. Lett. **102**, 017003 (2009).

[69] V. F. Maisi, S. V. Lotkhov, A. Kemppinen, A. Heimes, J. T. Muhonen, and J. P. Pekola, Excitation of Single Quasiparticles in a Small Superconducting Al Island Connected to

Normal-Metal Leads by Tunnel Junctions, Phys. Rev. Lett. **111**, 147001 (2013).

[70] K. L. Viisanen and J. P. Pekola, Anomalous electronic heat capacity of copper nanowires at sub-kelvin temperatures, Phys. Rev. B **97**, 115422 (2018).

[71] G. De Simoni, F. Paolucci, P. Solinas, E. Strambini, and F. Giazotto, Metallic supercurrent field-effect transistor, Nat. Nanotechnol. **13**, 802 (2018).

[72] B. Pannetier and H. Courtois, Andreev reflection and proximity effect, J. Low Temp. Phys. **118**, 599 (2000).